

# DualConv: Dual Mesh Convolutional Networks for Shape Correspondence

Nitika Verma<sup>1</sup> · Adnane Boukhayma<sup>2</sup> · Jakob Verbeek<sup>3</sup> · Edmond Boyer<sup>1</sup>

Received: date / Accepted: date

**Abstract** Convolutional neural networks have been extremely successful for 2D images and are readily extended to handle 3D voxel data. Meshes are a more common 3D shape representation that quantize the shape surface instead of the ambient space as with voxels, hence giving access to surface properties such as normals or appearances. The formulation of deep neural networks on meshes is, however, more complex since they are irregular data structures where the number of neighbors varies across vertices. While graph convolutional networks have previously been proposed over mesh vertex data, in this paper we explore how these networks can be extended to the dual face-based representation of triangular meshes, where nodes represent triangular faces in place of vertices. In comparison to the primal vertex mesh, its face dual offers several advantages, including, importantly, that the dual mesh is regular in the sense that each triangular face has exactly three neighbors. Moreover, the dual mesh suggests the use of a number of input features that are naturally defined over faces, such as surface normals and face areas. We evaluate the dual approach on the shape correspondence task on the FAUST human shape dataset and other versions of it with varying mesh topology. While applying generic graph convolutions to the dual mesh shows already improvements over primal mesh inputs, our experiments demonstrate that building additionally convolutional models that explicitly leverage the neighborhood size regularity of dual meshes enables learning shape representations that perform on par or better than previous approaches in terms of correspondence accuracy and mean geodesic error, while being more robust to topological changes in the meshes between training and testing shapes.

**Keywords** 3D Computer Vision · Geometric Deep Learning · Mesh Representation Learning · 3D Shape Modelling · Shape Correspondence

## 1 Introduction

The success of deep convolutional neural networks for recognition problems in 2D images (Krizhevsky et al. 2012; Simonyan and Zisserman 2015; He et al. 2016) has spurred a significant effort to transfer these results to the analysis of 3D shape data. One of the most direct approaches is to extend the 2D convolutions to 3D voxel grid shape representations (Maturana and Scherer 2015; Choy et al. 2016; Tatarchenko et al. 2017). Voxel grids are, however, inefficient in that they are extrinsic and quantize the modeling space, rather than the shape itself. While intrinsic representations such as point clouds and meshes are more attractive to model shapes, since they directly quantize the shape itself, the formulation of deep neural networks on such irregular structures is more complex. Point clouds provide a simple orderless data structure, and to be effective, networks for point cloud data often leverage an ad hoc notion of point proximity (Klokov and Lempitsky 2017; Qi et al. 2017b). In our work, we focus on 3D mesh representations, which offer a topological graph structure on top of the vertex positions allowing for a compact and accurate surface characterization.

The formulation of deep neural networks on meshes is not straightforward due to their irregular structure, where the number of neighbors can change from one vertex to another. A variety of different approaches to treating meshes as graphs has been explored in previous work. To deal with the irregular degree of the nodes, these methods use various assignment mechanisms to associate the neighbors with different filter weights, see e.g. (Monti et al. 2017; Verma

<sup>1</sup>Inria, Univ. Grenoble Alpes, CNRS, Grenoble INP, LJK, France

<sup>2</sup>Inria, Univ. Rennes, CNRS, IRISA, M2S, France

<sup>3</sup>Facebook AI Research, Paris, France

E-mail: firstname.lastname@inria.fr

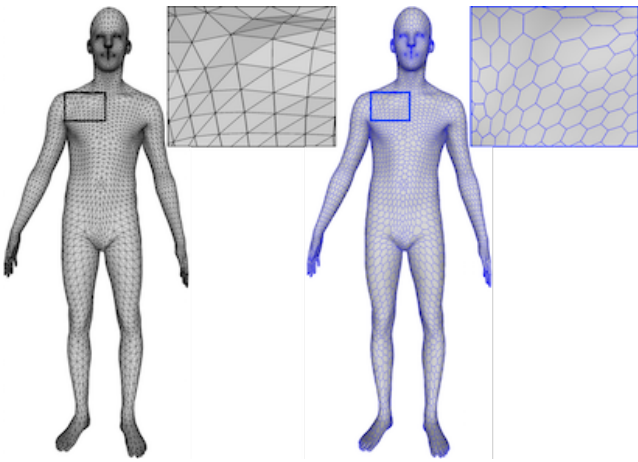


**Fig. 1** Illustration of a watertight triangular mesh (left) and its dual mesh defined on faces (right). Note that every vertex in the dual has exactly three neighbors, while the number of neighbors is not constant in the primal mesh (see top area of the left zoom).

et al. 2018; Fey et al. 2018). On the other hand, methods such as (Lim et al. 2018; Gong et al. 2019) use an explicit ordering of neighboring vertices to define convolutional operators. However, these methods do not take advantage of various geometric properties unique to meshes.

In this paper, we propose to use the dual mesh defined over the faces, where each vertex represents a face and is connected to the incident faces, see Figure 1. A watertight triangular mesh as an input ensures that each vertex in the dual mesh has exactly three neighbors. This allows us to define a regular convolution operator called DualConv on the dual mesh. Using the faces rather than the vertices to represent the data, it is also natural to use input features such as the face normal, or the area, among others, in combination with the location of the face center. We evaluate this convolution operator on the task of 3D shape correspondence between meshes. Since shape correspondence is typically defined over the mesh vertices rather than the faces, we introduce a dual-to-primal operator to map features from our dual-based network to the primal vertices, which can then be used to predict the correspondence.

We validate the feasibility of learning features in the dual domain and leveraging them for correspondence in the primal domain on the FAUST human shape dataset (Bogo et al. 2014), using merely the vertex/face center locations as input features on primal/dual meshes. We find that generic graph convolution methods improve in the dual domain compared to the primal, while our DualConv model –which additionally leverages the regularity of the dual mesh explicitly– performs even better.

Bogo et al. (2014) build the FAUST shape correspondence dataset by using texture information to align different meshes to a common template mesh, which results in all the shapes comprising of the same mesh topological vertices

and connectivity. We observe that this allows the previous work (Fey et al. 2018; Verma et al. 2018) to undesirably exploit local topological connectivity patterns, which is not exploitable in real-world settings where each shape will have a differently structured mesh. We advocate that our approach, based on regular three-neighbor dual meshes, eliminates the possibility to rely on local connectivity patterns to address the shape correspondence problem. To validate this hypothesis, we design more challenging evaluation setups for our approach while comparing to previous work and evaluating various additional input dual features.

First, we consider evaluating models trained on FAUST using decimated versions of it at various scales. This is a scenario where the structure of the test data gradually deviates from that of the training. Second, we train and test the models on a re-meshed version of FAUST (Ren et al. 2018), in a setup where the mesh structure varies both in training and testing. While being on par with the state-of-the-art on the second setup, our approach manages to preserve its initial performance through the increasing structural changes in the first setup considerably better than the existing approaches, specifically with face-based features, which implies that it succeeds in learning geometric and connectivity-independent representations. We also observe that the location and normal features are critical to obtaining accurate results. Moreover, we present qualitative results of correspondence learning transfer in-between the various aforementioned datasets when ground-truth is unavailable, including additionally the original raw FAUST scans. These visualizations confirm the numerical results.

In conclusion, our main contributions in this work can be summed up as follows:

- We propose to build a mesh-based regular convolution network on the face-based dual mesh.
- We propose a comparative evaluation of various input dual features and their combinations on the task of human shape correspondence.
- We demonstrate that the performance is better preserved by our dual approach compared to primal approaches under varying testing mesh topology.

In the next section, we review the most relevant related work. We then present our dual mesh approach in Section 3, followed by the presentation of experimental results in Section 4. Finally, we present our conclusions in Section 5.

## 2 Related work

In this section, we review related work on deep learning for the two most prominent explicit and intrinsic 3D shape representations, namely point clouds and meshes.

## 2.1 Deep learning on point clouds

Point clouds are a compact representation for 3D shapes that are widely adopted within many 3D visual reconstruction algorithms such as structure from motion and multi-view stereo, and 3D range sensors such as Kinect. PointNet (Qi et al. 2017a) paved the way for extending deep learning techniques for point clouds by using pointwise MLPs that process individual points, mixed with global operations across points built upon max-pooling. In order to incorporate geometric structures, PointNet++ (Qi et al. 2017b) proposes a network with local aggregation. Tree-based data structures like Octrees (Riegler et al. 2017) and K-d trees (Klokov and Lempitsky 2017) are used to learn features hierarchically. Li et al. (2018) propose a  $\chi$ -transformation to address the irregular and unordered nature of point clouds. DGCNN (Wang et al. 2019) uses edge convolution on graphs constructed dynamically from point clouds. For a more detailed review of these and other recent advances of deep learning in point clouds, we refer the reader to the survey paper of Guo et al. (2020). While point clouds are commonly used in shape acquisition pipelines, they do not provide an explicit representation of surfaces.

## 2.2 Deep learning on meshes

Meshes are an efficient representation for 3D shapes that approximate object surfaces with polygonal, often triangular, faces defined over a connected set of points. These data structures can also be considered as graphs embedded in  $\mathbb{R}^3$ , with nodes as the vertices and graph edges given by the edges of the faces. Recent techniques for deep learning on graphs can be categorized into spectral and spatial methods. We present a brief summary of these methods below and refer the reader to (Zhang et al. 2019; Wu et al. 2020) for more extensive reviews.

### 2.2.1 Spectral methods

Spectral graph convolutional networks are based on approaches from graph signal processing. Bruna et al. (2014) propose an extension of convolution for graphs using Laplacian Eigen-decomposition. In order to address the challenges posed by the high computational cost of this approach, Defferrard et al. (2016) propose to use Chebyshev K-polynomials for localized and efficient convolution filters. A simplified variant was introduced by Kipf and Welling (2017), using a first-order approximation of the Chebyshev expansion. Following these works, several other approaches (Levie et al. 2018; Chen et al. 2018; Huang et al. 2018) have been proposed. However, spectral-based methods do not generalize across domains with different graph structures. Consequently, they are mostly useful for inferring

node properties in situations where the graph during training and testing is the same (Sen et al. 2008; Ranjan et al. 2018; Bouritsas et al. 2019), and less suitable for tasks where different graphs are considered during training and testing (Ren et al. 2018; Hanocka et al. 2019).

### 2.2.2 Spatial methods

In contrast to spectral methods which operate globally, spatial methods compute features by aggregating information within local neighborhoods, similar to traditional CNNs. However, this is not straightforward because mesh graphs usually have irregular local structures: (i) the number of neighbors per node may vary, and (ii) even if the number of neighbors is fixed, there might not be a consistent ordering among them. To alleviate these challenges, patch-operator based methods (Masci et al. 2015; Boscaini et al. 2016) have been proposed where local patches are extracted using geodesic local polar coordinates and anisotropic heat kernels respectively. Monti et al. (2017) parameterize the patch-extraction by learning a mixture of Gaussian kernels associated with local polar pseudo-coordinates. Simonovsky and Komodakis (2017) dynamically generate convolutional filter weights conditioned on edge attributes neighboring the vertices. Fey et al. (2018) formulate convolutional filters based on B-spline basis functions, parameterized by learnt control values. Verma et al. (2018) proposed FeastNet which learns the mapping between convolutional filters and neighboring vertices dynamically using features generated by the network. Veličković et al. (2018) makes use of a multi-head attention mechanism to learn the association between two adjacent nodes.

### 2.2.3 Geometry-aware methods

In treating meshes as graphs, these methods do not leverage all the information which can be provided by meshes, in particular the arrangement in the 3D space of the vertices and faces. SpiralNet (Lim et al. 2018) construct a spiral operator which enumerates the neighboring vertices following randomly generated spiral patterns around the central vertex. A faster and more efficient extension of this approach is proposed in SpiralNet++ (Gong et al. 2019), where the spiral pattern is generated only once by assuming that all the meshes have fixed connectivity. MeshCNN (Hanocka et al. 2019) defines a convolution operation on edges aggregating information from their incident triangular edges. Furthermore, it proposes a task-driven pooling operation based on the edge-collapse operation (Hoppe 1997). One of the works most closely related to ours is that of Milano et al. (2020), which uses an attention-based approach on primal and dual graphs constructed from a triangular mesh. Their primal graph connects faces that share an edge, where the

dual graph connects edges that are part of the same face. They use a pooling operation based on edge contraction on the mesh. In contrast, we assume in our work that the vertices and edges of an input triangular mesh form the primal graph, and construct a dual mesh built on the faces. Rather than using a generic graph-based convolution on the dual mesh, we can therefore exploit the three-neighbor regularity to propose a dual mesh-based convolution. Additionally, we present an extensive evaluation of different features defined on faces and examine the ability to learn connectivity-independent representations using different approaches.

### 3 Method

We aim to benefit from the local geometric information encoded in a triangular mesh using deep learning models by applying convolution operations directly on this structure. The convolution operation hinges on the inductive bias stating that meaningful information can be extracted from a consistent input’s spatial local neighborhood. Typical convolutional networks are defined on regular grid-based images, where each pixel has ordered and equal number of neighbors. This allows to define a set of fixed-sized trainable filters that can be applied across the complete image. However, due to the irregular local structure of a mesh, it is difficult to define such filters in this case. We address this difficulty by designing convolution on the dual of triangular meshes, where each face has exactly three neighbors.

A primal mesh  $\mathcal{M}$  is defined by  $N_V$  vertices and  $N_F$  faces. The dual  $\mathcal{D}$  of  $\mathcal{M}$  is defined as a mesh where each vertex is centered on a face of  $\mathcal{M}$ . These vertices in the dual  $\mathcal{D}$  are connected by an edge if their corresponding two faces in the primal mesh  $\mathcal{M}$  share an edge. For a watertight mesh  $\mathcal{M}$ , where primal vertices can have different numbers of neighbors as shown in Figure 2, each vertex in the dual  $\mathcal{D}$  has exactly 3 neighbors by construction. In cases where the mesh  $\mathcal{M}$  is not watertight, we can use zero-padding to ensure that every vertex in  $\mathcal{D}$  has 3 neighbors. We note that in general, this approach can be extended to any  $N$ -edged polygonal mesh, where the face-based dual mesh will form a regular  $N$ -neighbor structure.

Our networks consist of two main building blocks. We introduce convolutional layers tailored explicitly for the fixed 3-neighborhood to process features on the dual mesh, and an operation to transfer features from the dual mesh back to the primal one, as required when the targeted output information is defined over the primal mesh vertices. This is the case for our task of interest: dense shape correspondence. As the network is defined over faces, we consider various input features characteristic of the latter.

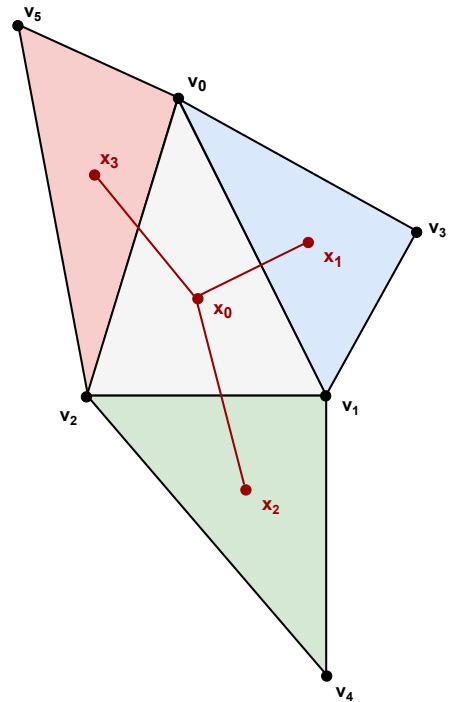


**Fig. 2** Illustration of the triangular face structure in primal mesh  $\mathcal{M}$  (in black) with vertices  $\{v_0, v_1, v_2, v_3, v_4, v_5\}$  and the corresponding dual mesh  $\mathcal{D}$  (in red) with vertices  $\{x_0, x_1, x_2, x_3\}$ . Note that the central vertex for  $\mathcal{D}$  has exactly three neighbors.

#### 3.1 Dual Convolution

Given a face in  $\mathcal{M}$ , represented by  $x_0$  in Figure 2, we wish to define the convolution as the dot product of the weights with the features of the neighbors, similar to a convolutional layer over regular pixel grids. Although the neighbors of a face can be assigned a unique clock-wise orientation defined w.r.t. the central face normal, their order is not unique (*i.e.* which neighbor comes first). To resolve the order ambiguity for the neighboring faces, we consider two different strategies inspired by previous work.

**DualConvMax.** This first strategy uses the surface normal to define neighbors’ orientation and mitigates their order ambiguity by max-pooling over application of the filter, treating each one of the neighbors as the first, analogously to angular max-pooling (Masci et al. 2015). Let  $C_I$  and  $C_O$  denote the number of feature channels in the input and output of the convolution respectively. The central node’s feature  $x_0$  is always multiplied with the same weights  $\mathbf{U} \in \mathbb{R}^{C_O \times C_I}$ . Weights  $\mathbf{W} \in \mathbb{R}^{C_O \times 3C_I}$  are applied to the local neighbors using their three possible orderings, followed by a coordinate-wise max-pooling across the orders:

$$y_0 = \mathbf{U}x_0 + \max\{\mathbf{W}x_{1,2,3}, \mathbf{W}x_{2,3,1}, \mathbf{W}x_{3,1,2}\}, \quad (1)$$

where  $y_0 \in \mathbb{R}^{C_O}$  is the output feature,  $x_{1,2,3} \in \mathbb{R}^{3C_I}$  denotes the concatenation of the neighbors  $x_1, x_2$  and  $x_3$  in this order.

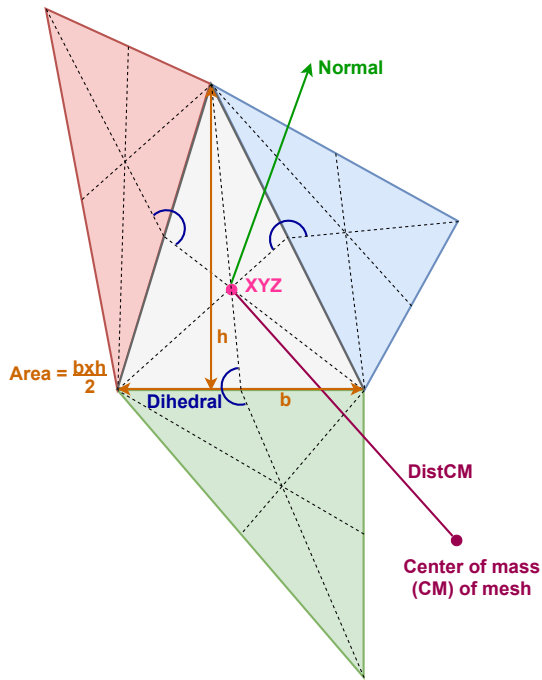


Fig. 3 Illustration of input features defined on the dual mesh.

**DualConvInv.** The second strategy follows the same principle as in Hanocka et al. (2019). We define a symmetric function on the input features to create order and orientation invariant features  $\mathbf{f} \in \mathbb{R}^{3C_I}$  for the neighborhood  $\{x_1, x_2, x_3\}$  of  $x_0$ :

$$\mathbf{f} = \begin{pmatrix} x_1 + x_2 + x_3, \\ [x_1 - x_2]^+ + [x_2 - x_3]^+ + [x_3 - x_1]^+, \\ [x_2 - x_1]^+ + [x_3 - x_2]^+ + [x_1 - x_3]^+ \end{pmatrix}, \quad (2)$$

where  $[a]^+ = \max(0, a)$ . These features are used together with the central node to compute the convolution output:

$$y_0 = \mathbf{U}x_0 + \mathbf{W}\mathbf{f} \quad (3)$$

### 3.2 Dual to Primal Feature Transfer

In many applications the prediction targets and/or the ground-truth for training is defined on the vertices of the primal mesh only. To handle such cases, we define a **Dual2Primal** layer to transfer the features from the dual back to the original mesh. The features transferred to the primal mesh can then be used to measure the loss for training, or to make predictions for evaluation.

Given a mesh  $\mathcal{M}$ , we construct a vertex-face adjacency matrix  $\mathbf{A} \in \mathbb{R}^{N_V \times N_F}$ , and derive the vertex-degree matrix  $\mathbf{D} = \text{diag}(\mathbf{A}\mathbf{1}_{N_F})$ , where  $\mathbf{1}_{N_F}$  is a vector of ones of size  $N_F$ . The diagonal of  $\mathbf{D}$  contains for each vertex in the primal mesh the number of faces to which it belongs. The output features  $\mathbf{F}_{Dual}$  obtained using the dual neural network

Input	Translation	Rotation	Scale
XYZ	×	×	×
Normal	✓	×	✓
Area	✓	✓	×
DistCM	✓	✓	×
Dihedral	✓	✓	✓

Table 1 Invariances provided by features defined on the dual mesh.

are converted into features  $\mathbf{F}_{Primal}$  on the primal mesh by averaging for each vertex of the primal mesh the features obtained from the dual network of all faces incident to that vertex:

$$\mathbf{F}_{Primal} = \mathbf{D}^{-1} \mathbf{A} \mathbf{F}_{Dual}. \quad (4)$$

We then apply the loss defined on the primal mesh and back-propagate the gradients through the dual network.

### 3.3 Input Dual Features

Using faces rather than vertices as inputs for our deep network allows the use of features that are naturally defined over faces but not over vertices, such as face normals, face areas, or angles between faces. In our experiments, we explore the effectiveness of a variety of different input features defined for faces including:

- **XYZ**: the coordinates of the center of mass of the face.
- **Normal**: the unit vector in the direction of the face normal.
- **Dihedral**: the angles (in radians) between the face and its neighbors.
- **Area**: the surface area of the face.
- **DistCM**: the Euclidean distance between the center of mass of the full mesh and the face.

We illustrate these features in Figure 3. Table 1 lists the different invariances offered by each, ranging from XYZ that does not offer any invariance, to dihedral angles which are invariant to translation, rotation, and scaling of the 3D shape. We note that the dihedral angles are defined per adjacent face, so we use them by setting  $x_0 = 0$  and  $x_i = \text{Dihedral}_{0,i}$  in Equations 1, 2 and 3. As the remaining features are defined per face, we can directly use them as inputs following the former equations. In our experiments, we also consider combinations of these features, by concatenating them into a larger input feature.

## 4 Experimental evaluation

In this section, we first describe our experimental setup in Section 4.1. We then present our experimental results when

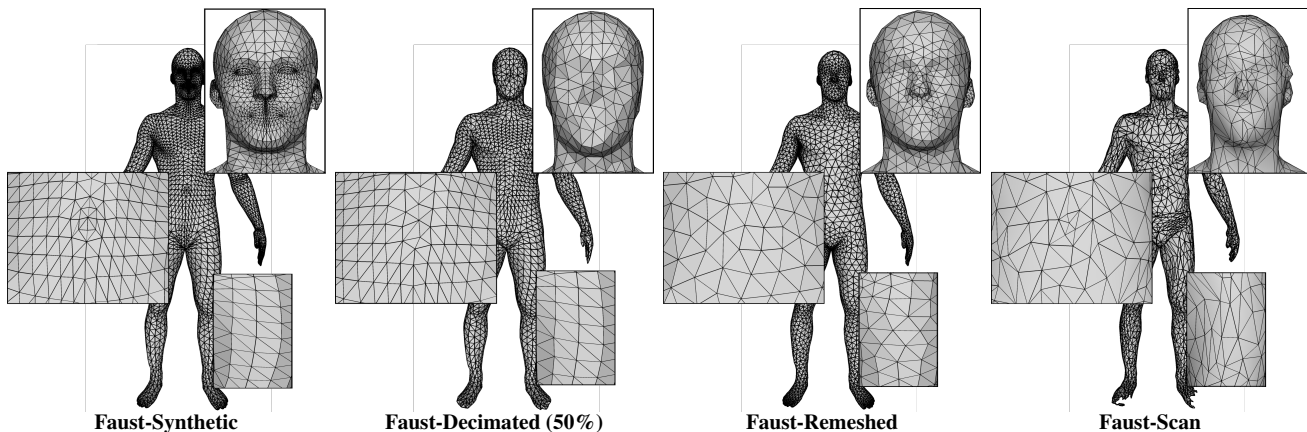


**Fig. 4** Visualizations of a FAUST test mesh from the template-fitted dataset, decimated at 50% resolution, re-meshed version and original scan.

training our models on the FAUST and re-meshed FAUST datasets in sections 4.2 and 4.3 respectively.

#### 4.1 Experimental setup and implementation

We closely follow the experimental setup of previous work (Monti et al. 2017; Verma et al. 2018; Fey et al. 2018) on the FAUST dataset. In addition, for a more realistic evaluation accounting for mesh topological change, we extend experiments to other versions of FAUST, namely decimated versions of it, a re-meshed version of it, and its original scans (see Figure 4). Below, we describe these datasets, the network architectures and training, as well as the evaluation metrics in detail.

##### 4.1.1 Datasets

We perform evaluations on the FAUST human shape dataset (Bogo et al. 2014). The version of the dataset used in prior work (Monti et al. 2017; Verma et al. 2018; Fey et al. 2018) contains 100 watertight triangular meshes, in which there are 10 shapes of as many different people, with each shape striking 10 different poses. We use the first 80 meshes for training and the last 20 meshes for testing. The meshes in the dataset are obtained by fitting a fixed template mesh with 6,890 vertices and 13,776 faces each to raw scan data. We refer to this dataset as “Faust-Synthetic” in the evaluations. All meshes have the same underlying connectivity, and the ground-truth is defined by a one-to-one correspondence of the vertices.

To allow for more challenging evaluations with varying mesh topologies, we consider three other versions of the dataset. First, we use quadric edge collapse decimation (Garland and Heckbert 1997) to reduce the resolution of the meshes in Faust-Synthetic by up to 50%. Edges are selected to be collapsed in order of increasing lengths. We refer to this version of the dataset as “Faust-Decimated”.

While mesh decimation is a fairly straightforward way to assess robustness to changes in the mesh structure, we note that it changes some parts of the mesh more drastically than others. We visualize this in Figure 4, where we observe substantial changes over the face, but the legs are barely affected. Moreover, we observe that decimation leads to substantial loss of detail in denser areas like the face, where key features are missing.

Second, we consider the re-meshed version of the dataset introduced by Ren et al. (2018) as a more realistic and challenging testbed. It was obtained by re-meshing every shape in the Faust-Synthetic dataset independently using the LRVD method (Yan et al. 2014). Each mesh in the resulting dataset consists of around 5,000 vertices and has a unique mesh topology. While offering an interesting testbed, the re-meshed data does not come with dense one-to-one vertex ground-truth correspondence. A partial ground-truth is however available for roughly 3,500 vertices. We refer to this dataset as “Faust-Remeshed” below.

Finally, we also consider the raw scan data that underlies the dataset. It contains 200 high-resolution meshes, with the same 10 people striking 20 different poses. The average number of vertices in each scan is around 172,000, which we reduce using quadric edge collapse decimation (Garland and Heckbert 1997) to bring closer to the reference template with 6,890 vertices. We note that this dataset is very challenging as it does not contain watertight meshes and all meshes have different topologies. There is no ground-truth available, so we only perform a qualitative evaluation on this version of the dataset. We refer to this dataset as “Faust-Scan” in our experiments. In Figure 4 we illustrate the different versions of the data for one example mesh.

##### 4.1.2 Network architectures and training

Figure 5 describes the dual mesh-based architecture that we use in our experiments, where  $N_V$  and  $N_F$  are the number of vertices and faces in the original primal mesh respectively,

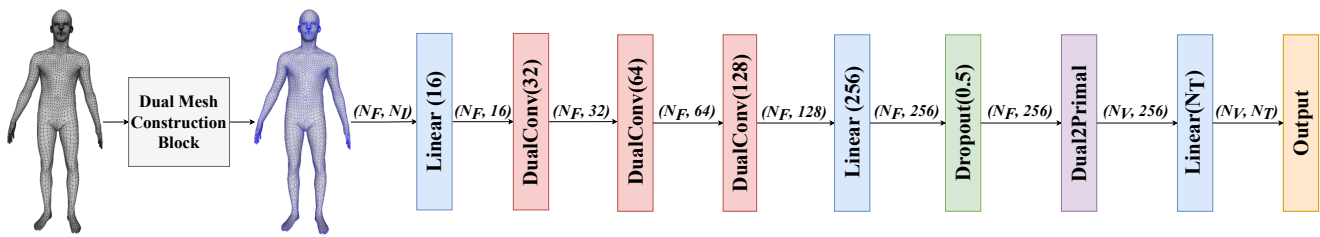


Fig. 5 Our network architecture for dual meshes. For FeaStNet–Dual, we use the same architecture by replacing DualConv with FeaStConv.

$N_T$  the number of target labels and  $N_I$  the number of input features. We use “Linear( $K$ )” to indicate fully connected layers, and “DualConv( $K$ )” to indicate graph-convolutional layers (defined in Section 3.1), producing each  $K$  output feature channels. “( $N, K$ )” denotes feature maps of size  $N$  and dimension  $K$ . We apply the Exponential Linear Unit (ELU) non-linearity (Clevert et al. 2016) after every DualConv layer and every linear layer, except for the last one. We also indicate the dropout rate for the Dropout layer (Srivastava et al. 2014).

Similar to previous work (Monti et al. 2017; Verma et al. 2018; Fey et al. 2018), we formulate the shape correspondence task as a vertex labeling problem, where the labels are the set of vertices in a given reference shape. We implemented our method using the PyTorch Geometric framework (Fey and Lenssen 2019). We train models using the Adam optimizer (Kingma and Ba 2015) to minimize the cross-entropy classification loss.

We train the competing methods MoNet (Monti et al. 2017), SplineCNN (Fey et al. 2018) and FeaStNet (Verma et al. 2018) ourselves in our various evaluation setups using the PyTorch Geometric framework (Fey and Lenssen 2019). We use the same base architecture for primal and dual based methods alike as given in Figure 5, where we replace the DualConv blocks with the corresponding convolutional blocks. We use SHOT descriptors (Tombari et al. 2010) as input features for MoNet, and XYZ for SplineCNN and FeaStNet. While our DualConv operators have three weights per filter by construction, due to the regularity of the dual mesh, for the other methods the number of weights is a hyperparameter. In our experiments, we use the same number of weights per filter as in the original papers, *i.e.* 8 for FeaStNet and FeaStNet–Dual (FeaStNet applied to the dual mesh) and 5 for SplineCNN.

Table 2 shows the average execution time of a forward pass for a mesh of the re-meshed FAUST dataset for the different models used in our experiments on a Tesla P100 GPU, as well as the number of parameters of these models. All methods have a comparable number of parameters and execution times except SplineCNN. It takes roughly twice longer to complete a forward pass, and possesses roughly twice as many parameters as the other methods. For MoNet, the forward pass time does not include the computation of

Mesh Domain	Method	Time (in ms)	#Params
Primal	MoNet	$8.9 \pm 0.25$	1.4M
	SplineCNN	$17.8 \pm 0.15$	3.1M
	FeaStNet	$10.6 \pm 0.17$	1.4M
Dual	FeaStConv–Dual	$10.4 \pm 0.14$	1.4M
	DualConvMax	$8.6 \pm 0.57$	1.3M
	DualConvInv	$9.4 \pm 0.16$	1.3M

Table 2 Comparison of the number of parameters and average execution time of the forward-pass per mesh for Faust-Remeshed dataset.

the SHOT descriptors, which are used as input to the model, and take an additional 400 ms to compute per mesh on CPU.

#### 4.1.3 Evaluation metrics

Following previous work (Monti et al. 2017; Verma et al. 2018; Fey et al. 2018), we report the accuracy, *i.e.* the fraction of vertices for which the exact correspondence has been correctly predicted. Assuming correct correspondences for predictions with geodesic distances to the ground-truth below a given threshold, we also plot the percentage of correct predictions as a function of this geodesic threshold, that we express both in cm and normalized by a diameter of 200cm. In addition, we report the mean geodesic error, *i.e.* the average of the geodesic distance between the ground-truth and the prediction, normalized by the geodesic diameter and multiplied by 100. We believe the mean geodesic error metric is more informative than the accuracy as a single-number comparison for the correspondence task, since rather than just counting the correspondence mistakes, it takes into account how large the correspondence errors are.

## 4.2 Experimental results on the Faust-Synthetic dataset

Using the Faust-Synthetic dataset, we first validate the use of the dual mesh for shape correspondence in Section 4.2.1 with just XYZ positions as input features. After this validation under the simplified setting of fixed mesh structure across shapes, we continue with more challenging experiments where we test on meshes with different topologies. In

Mesh	Method	Input	Mean Geo. Error	Accuracy
Primal	FeaStNet	XYZ	1.39	88.1%
	FeaStNet-Dual	XYZ	0.18	92.7%
Dual	DualConvMax	XYZ	0.26	95.5%
	DualConvInv	XYZ	0.23	89.1%

**Table 3** Mean geodesic error and correspondence accuracy. Comparing primal and dual methods on the Faust-Synthetic dataset.

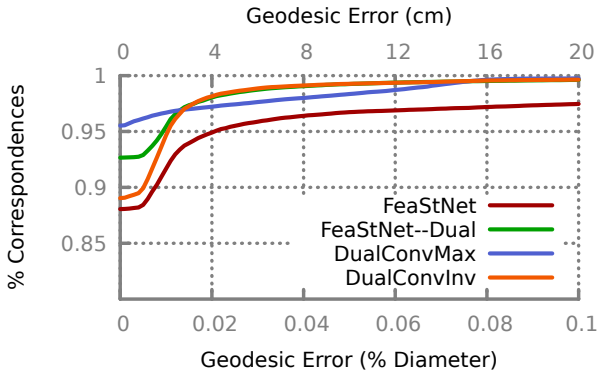


**Fig. 6** Percentage of correct shape correspondences within a certain geodesic distance to the ground truth, comparing primal and dual methods on the Faust-Synthetic dataset.

Section 4.2.2 we explore the effectiveness of different features that are available on the dual mesh, and in Section 4.2.3 we compare to previous work. We present a qualitative evaluation of the transfer of models trained on Faust-Synthetic to the completely restructured meshes in Faust-Scan and Faust-Remeshed in Section 4.2.4.

#### 4.2.1 Validation of networks trained on the dual mesh

The shape correspondence task on the FAUST dataset is defined on the mesh vertices. In our first experiment, we validate the use of the dual mesh to establish shape correspondence, and the effectiveness of networks built on our DualConv (Section 3.1) and Dual2Primal (Section 3.2) operators. For this purpose, we use the XYZ position of the face centers as input and compare results to those obtained with FeaStNet (Verma et al. 2018) on the primal mesh. Since FeaStNet is a generic graph convolution method, it can be readily applied to the dual mesh. We refer to the results obtained using this approach as FeaStNet-Dual. This allows us to separate the effects of using the primal vs. dual mesh from and the use of our DualConv layers.

We present the results in Table 3. Comparing FeaStNet and FeaStNet-Dual, we observe that the Dual2Primal layer successfully transfers features learned over the faces to the primal vertices. Moreover, using the dual mesh improves performance: the mean normalized geodesic error drops from 1.39 to 0.18, and the accuracy increases from

88.1% to 92.7%. Next, we evaluate our DualConvMax and DualConvInv layers which are defined explicitly for the dual mesh. Both of our methods perform better than FeaStNet in terms of accuracy and mean geodesic error. With regard to mean geodesic error they are slightly worse than FeaStNet-Dual, while DualConvMax obtains the highest overall accuracy (95.5%). DualConvInv performs worse than both these methods in terms of accuracy and intermediate in terms of geodesic error. Note that all dual-based approaches are better than FeaStNet in terms of accuracy and obtain much lower mean geodesic errors. The accuracy as a function of geodesic distance to the target is presented in Figure 6, confirming the improved correspondence prediction using the dual mesh.

Based on these encouraging results, we now turn to evaluations in more challenging conditions. The Faust-Synthetic dataset is unrealistic in that all meshes share one identical mesh structure connectivity. Therefore, it is possible that deep networks that are trained on them learn to exploit this property to solve the correspondence problem on this dataset, without being able to generalize to shapes with other mesh topologies. To assess to what extent this happens, in the experiments below we train the networks on Faust-Synthetic and test the resilience to connectivity changes on Faust-Decimated.

#### 4.2.2 Feature evaluation

We compare the effectiveness of the different input features on the dual mesh, described in 3.3, for networks built on both our DualConvMax and DualConvInv operators. In preliminary experiments, we observed that using XYZ in input features is essential for obtaining good performance on the Faust-Synthetic dataset. We therefore only report results on feature combinations which include XYZ.

In Figure 7, we plot the accuracy and mean geodesic errors on test meshes ranging from no reduction to 50% reduction of the original resolution. We first discuss the results on test meshes without decimation (the leftmost point on the curves). We observe that all feature combinations achieve similar mean geodesic errors, but that in terms of accuracy just XYZ gives the best results. We observe that DualConvInv performs worse than DualConvMax for all input feature combinations in terms of accuracy.

We now compare how these features perform as we decimate the meshes up to 50% of their original resolutions. Overall, the results obtained with DualConvMax are better than those obtained with DualConvInv. For DualConvMax, the combination of XYZ+Normal and XYZ+Normal+Dihedral+DistCM are best in terms of mean geodesic error. While just XYZ is best in terms of accuracy, for the 50% decimation setting it is suboptimal in terms of mean geodesic error. Adding the area feature to

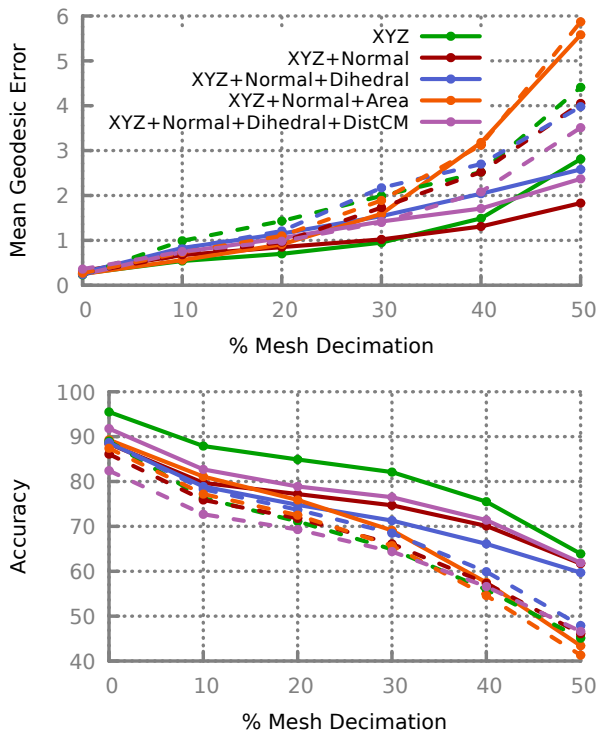


**Fig. 7** Shape mean normalized geodesic error and correspondence accuracy for Faust-Decimated test meshes. Solid lines represent DualConvMax, dashed lines represent DualConvInv. All networks are trained on the full resolution Faust-Synthetic meshes using different input features given in the legend at the top.

XYZ+Normal degrades the performance considerably because decimation leads to big changes in local face areas. Based on these conclusions, we only consider the best performing XYZ+Normal and XYZ features using DualConvMax in comparison to primal methods below.

#### 4.2.3 Comparison to previous work

We compare our approach with the previous state-of-the-art methods in Figure 8. We observe that the networks that use the dual mesh are more robust to connectivity changes than MoNet, SplineCNN and FeaStNet which are based on the primal mesh. Using XYZ as input features, our DualConvMax improves the accuracy by 2.8% as compared to FeaStNet applied to the dual (FeaStNet-Dual) in the case without connectivity changes, and leads to substantially better accuracy of 63.9% compared to the 44.2% when meshes are decimated by 50%. We note that the methods on the primal mesh all achieve poor mean geodesic errors on the decimated meshes. Taking into account the results obtained with FeaStNet-Dual, we note that the improved performance of DualConvMax w.r.t. previous methods (MoNet, SplineCNN and FeaStNet) is both due to the use of the dual mesh structure and to the DualConvMax operators that we designed for the dual mesh.

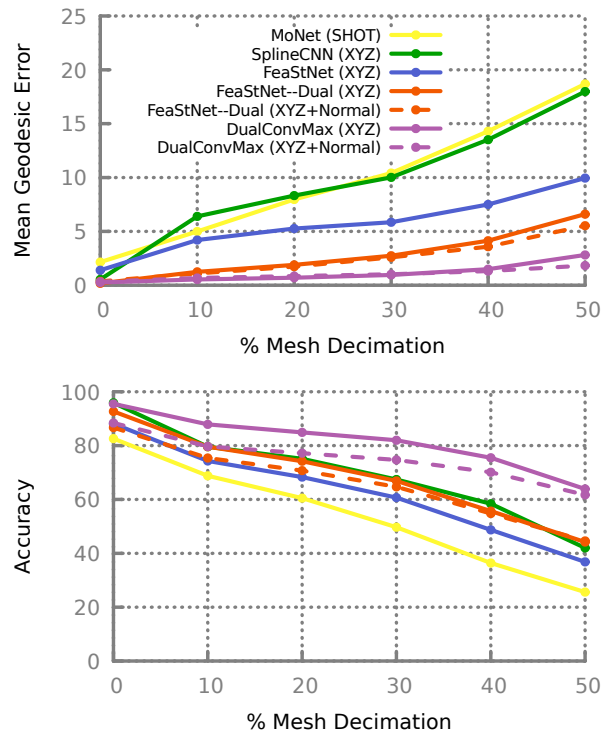


**Fig. 8** Shape mean geodesic error and correspondence accuracy for Faust-Decimated test meshes with XYZ. All methods are trained on the original full resolution meshes.

We qualitatively compare the results of MoNet, SplineCNN and FeaStNet on the primal, FeaStNet-Dual and our DualConvMax using texture transfer and geodesic errors in Figure 9 for an example non-decimated test mesh and its 50% decimated version. We observe marked improvements in the results on the reduced mesh by using the dual rather than primal mesh, and further substantial improvements by using our DualConvMax approach rather than FeaStNet-Dual using both XYZ and XYZ+Normal features. This confirms what was observed in terms of the accuracy and mean geodesic error metrics before.

#### 4.2.4 Qualitative results on Faust-Scan and Faust-Remeshed

Above we observed that the approaches based on the dual mesh are more robust to topological changes induced by mesh decimation. We now turn to a qualitative evaluation on the Faust-Scan and Faust-Remeshed datasets. In these datasets, the topological changes appear across the complete shape, where the mesh decimation only has a local effect and can leave part of the meshes intact. We again train our models on the Faust-Synthetic dataset. Since there is no ground-truth correspondence across these different versions of the dataset, we only present qualitative results using tex-

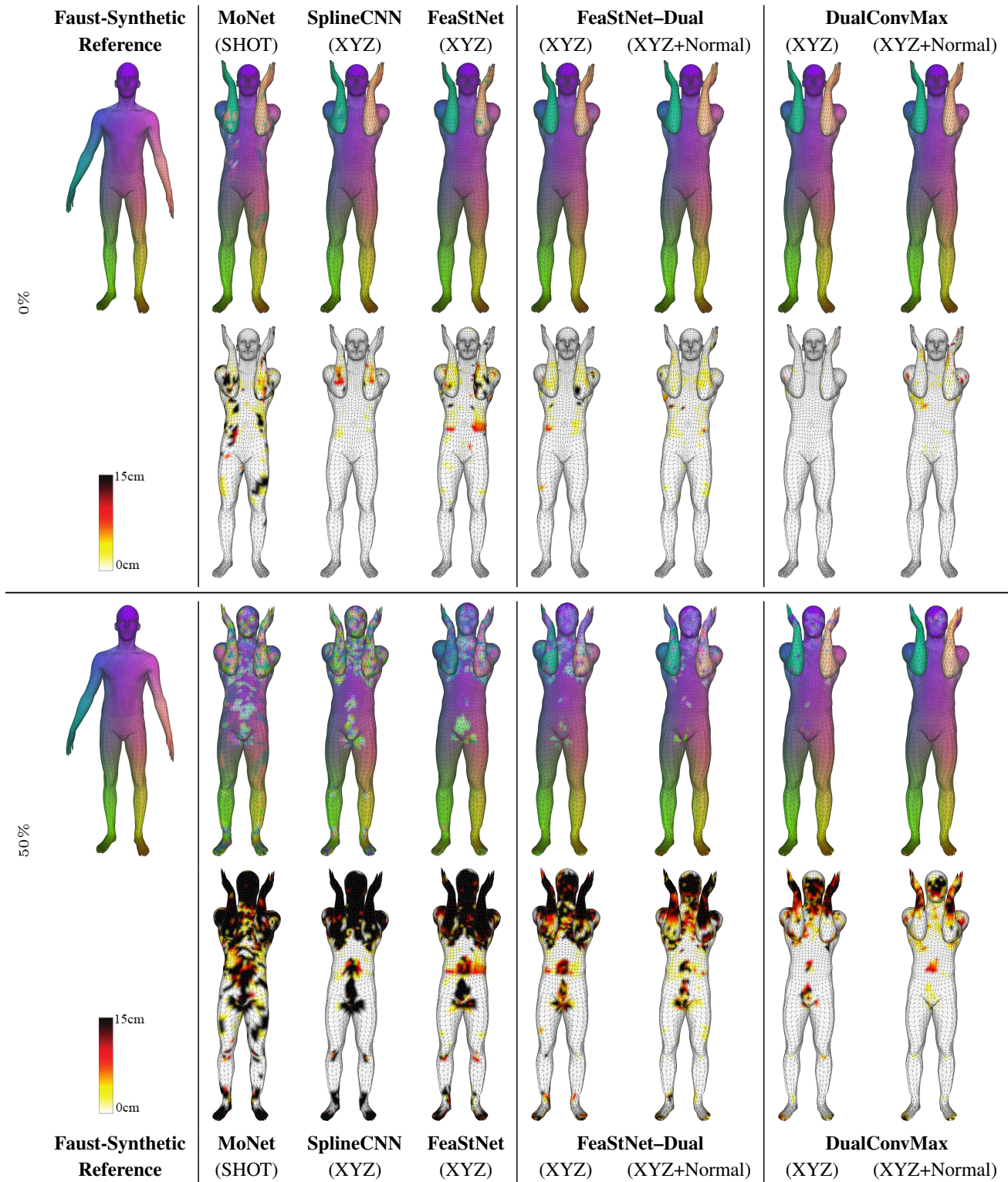


**Fig. 9** Visualizations of texture transfer and geodesic correspondence errors for a full resolution Faust-Synthetic test mesh (top two rows), and the same mesh decimated by 50% (bottom two rows) of the Faust-Decimated dataset. Models are trained on the full resolution Faust-Synthetic meshes.

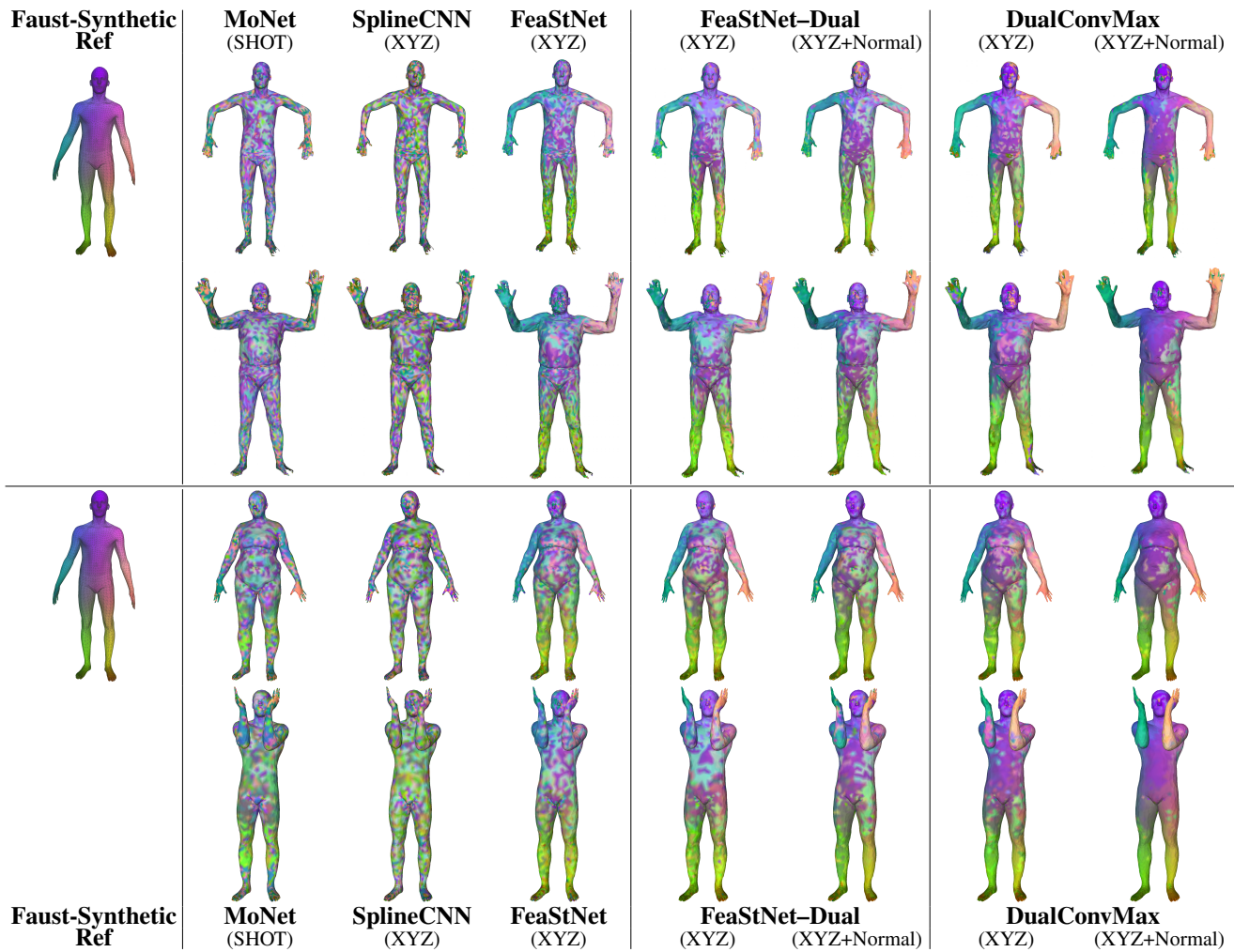


**Fig. 10** Visualizations of texture transfer for Fausta-Scan test results in the first two rows and Fausta-Remeshed in the last two rows. All methods have been trained on the Fausta-Synthetic dataset.

texture transfer from the Fausta-Synthetic reference mesh to the test meshes.

We compare MoNet, SplineCNN and FeaStNet on primal meshes to FeaStNet-Dual and our DualConvMax approach on dual meshes in Figure 10. These texture transfer results show that the correspondence problem for these shapes is substantially harder than that for the decimated meshes. The methods based on the primal mesh fail to recover most correspondences. FeaStNet-Dual recovers more correspondences, but is overall still very noisy. With our DualConvMax approach, we obtain significantly cleaner transfer results, in particular when adding the Normal features. This results show that our DualConvMax approach learns shape representations that do not rely on the fixed mesh topology of the training meshes, and that is thus more robust to changes in the mesh.

#### 4.3 Experimental results on Fausta-Remeshed

In the experiments so far, none of the methods were exposed to structural changes in the meshes during training on Fausta-Synthetic. We observed that the primal-based methods failed to generalize to the substantially differently structured meshes in the Fausta-Remeshed and Fausta-Scan datasets, while our DualConvMax approach is still able to obtain reasonable results using the XYZ+Normal features (*c.f.* Figure 10). In this section, we consider to what extent the different methods can be trained to be robust to such topological changes, by training the models on the Fausta-Remeshed dataset, where each shape has a unique mesh structure.

We study the different dual features and their combinations using our DualConv method in this setting in Section 4.3.1. We compare with previous methods in Section 4.3.2, and present qualitative evaluation on Fausta-Scan meshes in Section 4.3.3.

Input	Translation	Rotation	Scale	DualConvMax		DualConvInv	
				Mean Geo. Error	Accuracy	Mean Geo. Error	Accuracy
XYZ	×	×	×	1.8	37.3%	1.4	41.8%
Normal	✓	×	✓	7.1	40.3%	7.2	39.7%
Area	✓	✓	×	27.1	10.6%	27.8	9.5%
Dihedral	✓	✓	✓	22.6	15.7%	22.9	15.3%
DistCM	✓	✓	×	18.1	14.7%	19.9	10.9%
XYZ+Normal	×	×	×	<b>1.3</b>	45.8%	<b>1.1</b>	48.3%
Normal+DistCM	✓	×	×	2.4	48.3%	2.3	47.1%
Normal+Area+DistCM	✓	×	×	2.5	<b>49.2%</b>	2.1	<b>48.4%</b>
Normal+Dihedral	✓	×	✓	6.3	41.3%	6.4	41.4%
Dihedral+Area+DistCM	✓	✓	×	13.4	28.9%	14.5	25.9%

**Table 4** Mean geodesic errors and correspondence accuracy for DualConv using different input features on Faust-Remeshed meshes.

Mesh Domain	Method	Input	Mean Geo. Error	Accuracy
Primal	MoNet	SHOT	4.1	<b>48.7%</b>
	SplineCNN	XYZ	7.2	39.7%
	FeaStNet	XYZ	1.6	47.6%
Dual	FeaStNet--Dual	XYZ	1.7	37.8%
		XYZ+Normal	1.5	42.4%
	DualConvMax	XYZ	1.8	37.3%
		XYZ+Normal	1.3	45.8%
	DualConvInv	XYZ	1.4	41.8%
		XYZ+Normal	<b>1.1</b>	48.3%

**Table 5** Mean geodesic errors and correspondence accuracies using state-of-the-art methods on primal/dual meshes and using our best performing methods/input features for the Faust-Remeshed dataset.

### 4.3.1 Feature Evaluation

First, we evaluate the impact of using different input features and their combinations described in 3.3 in the current setting. We study the performance of each feature individually in the upper part of Table 4, and in the lower part, we compare different feature combinations, by combining the features which perform best individually.

Overall, comparing the two dual architectures we developed, we observe similar trends in performance across the features. DualConvMax generally leads to higher accuracy, except for settings where we include the XYZ features. The face normal and XYZ location of the face center provide similar accuracy, well above results obtained using other features. While face normals offer translation and scale invariance, the geodesic error is higher as compared to XYZ. The combination of XYZ and face normals improves over their individual performances and obtains the smallest geodesic error, but does not offer any invariance.

Among the features which provide translation invariance, we combine Normal and DistCM, which encodes the plane in which the face lies. This translation-invariant feature combination yields similar accuracy as the

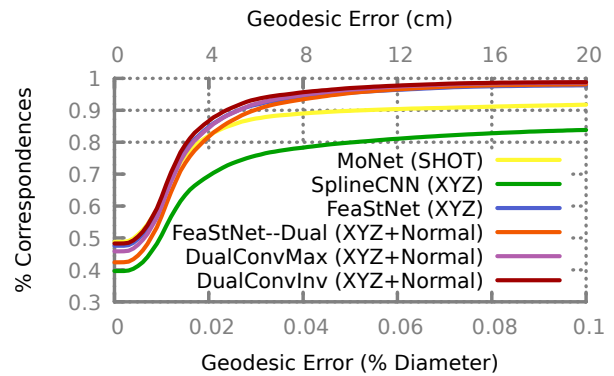


**Fig. 11** Percentage of correct shape correspondences within a certain geodesic distance to the ground truth, using state-of-the-art methods on primal/dual meshes and using our best performing methods/input features for the Faust-Remeshed dataset.

XYZ+Normal combination, but yields higher geodesic errors. To further add translation-invariant face information we add the area feature. This further boosts the accuracy for both the DualConvMax and DualConvInv architectures and achieves the best performance in terms of accuracy. Similarly, we test the combinations Normal+Dihedral and Dihedral+Area+DistCM. Both of these combinations offer an advantage of translation invariance plus scale invariance in the former, and rotation in the latter, but lead to reduced accuracy and higher geodesic error using both the DualConvMax and DualConvInv architectures.

### 4.3.2 Comparison to previous work

In Table 5, we compare our DualConvMax and DualConvInv models with previous state-of-the-art models. MoNet uses SHOT local shape descriptor features as input, while other models use elementary XYZ features or combine these with the face normals. Using the XYZ location features, FeaStNet on dual performs worse compared to using these features on the primal mesh in terms of accuracy, however,

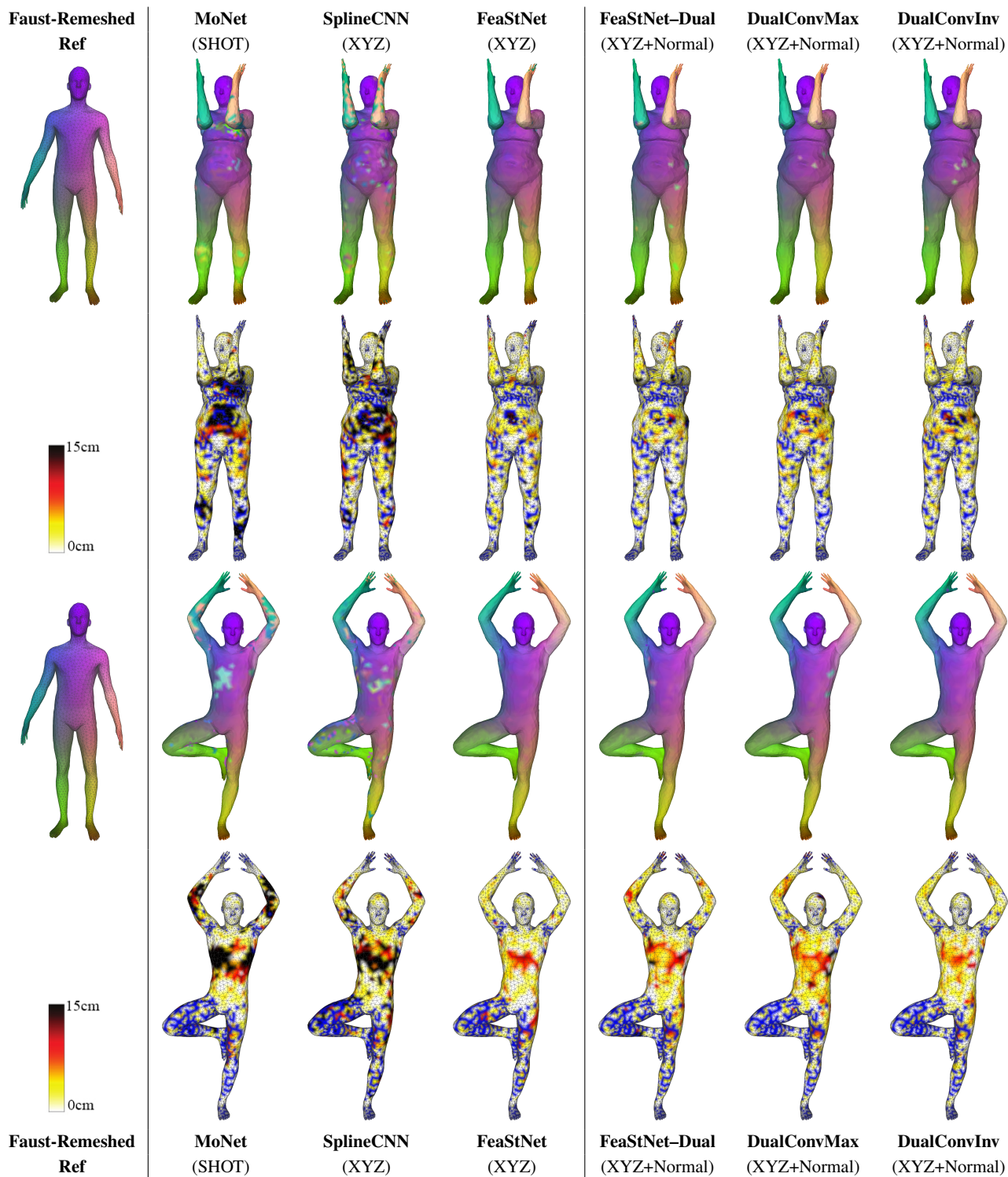


**Fig. 12** Visualizations of texture transfer for Faust-Remeshed test results trained on Faust-Remeshed dataset using the state-of-the-art methods and our method. The vertices for which the ground-truth is missing are colored blue in the error meshes.

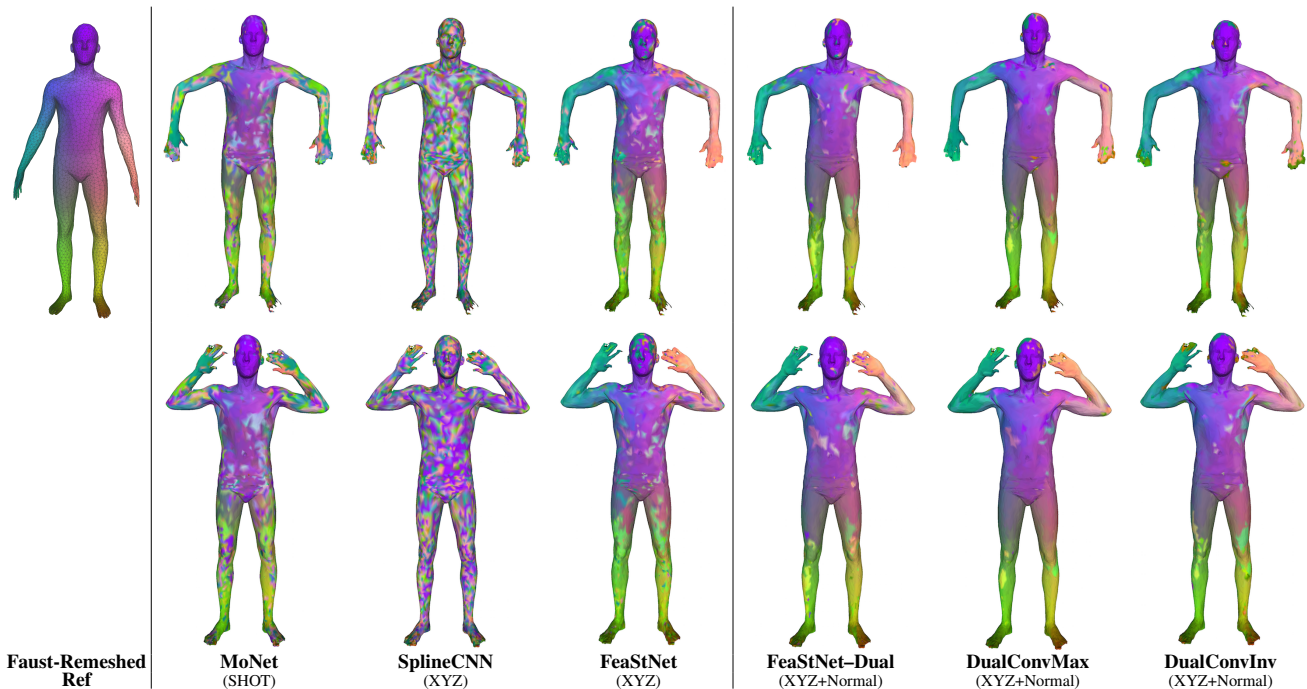


**Fig. 13** Visualizations of texture transfer for Faust-Scan results for models trained on the Faust-Remeshed dataset using primal and dual meshes.

the geodesic error is similar. Including the face normal features for the dual approaches leads to substantial improvements in accuracy for all three methods tested in the dual domain, and also reduces the mean geodesic errors for all of them. Our DualConv models give comparable accuracy and lower geodesic errors compared to state-of-the-art models in the primal domain.

We present a comparison of accuracy as a function of geodesic distance to the target for these methods in Figure 11. For clarity of presentation, we only display results for the XYZ+Normal feature combination for the dual methods. The results confirm what was observed in Table 5.

We provide qualitative evaluations in Figure 12. We visualize the texture transfer from the Faust-Remeshed reference shape to Faust-Remeshed test shapes and correspondence errors for these methods in Figure 12. Due to the partial ground-truth on re-meshed meshes, we represent the vertices for which the ground-truth is missing as blue in the error meshes. Once exposed to structural mesh changes during training, we observe that primal-based methods perform much better than when they were trained on Faust-Synthetic (*c.f.* Figure 10). In particular, FeaStNet is able to obtain results that are roughly comparable to the results obtained using the dual-based methods.

#### 4.3.3 Qualitative evaluation on Faust-Scan

Finally, we evaluate all methods trained on the Faust-Remeshed data and visualize texture transfer to the Faust-Scan meshes in Figure 13. We observe that training on re-

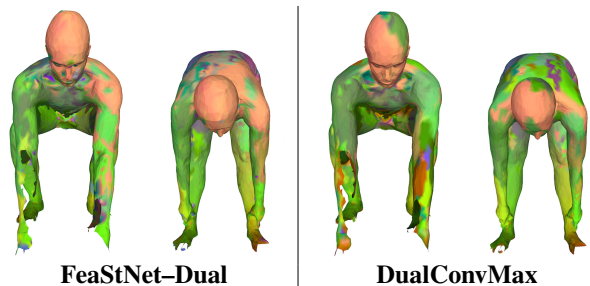


**Fig. 14** Visualizations of results from Faust-Scan trained on the Faust-Remeshed dataset using XYZ+Normal as input features.

meshed versions of the shapes helps to make primal methods MoNet and FeaStNet more robust to topological changes. However, we observe that SplineCNN (also primal) is not able to generalize to topologically different meshes even after training on re-meshed versions. Also in this setting, the dual-based methods generalize best to differently structured meshes.

Failure modes of the dual-based models tend to appear on test poses in Faust-Scan that are very different from the training poses in Faust-Remeshed. We show two such instances in Figure 14. In particular, the bent pose is problematic for the correspondences for the upper body.

## 5 Conclusion

We explored the use of the dual mesh to learn shape representations for 3D mesh data as an alternative to the more

commonly used primal mesh. Performing convolution operations in the dual domain presents the advantage of the neighborhood size being fixed, and allows access to input features defined naturally on faces such as normals and face areas. We focused our experimental study on the task of real human shape dense correspondence using the FAUST human shape dataset. We introduced two convolutional operators for the dual mesh, and benchmarked them using multiple input features based on the dual mesh.

In our experiments, we compare our dual mesh approaches to existing methods based on the primal mesh, and also apply the generic graph convolutional approach FeaStNet on the dual mesh. Through experiments where we train on one version of the dataset and test on another version of the dataset with different mesh topology, we assess the robustness of different models to such topological changes. We find that primal methods trained on the Faust-Synthetic dataset, with constant mesh topology across shapes, are very brittle and generalize poorly to meshes with different topologies. This can be remedied to some extent by training on meshes with varying topology, as we did using the Faust-Remeshed dataset. Our results show the robustness of our convolutional operators applied on the dual mesh, by achieving the best performances when testing on structurally different meshes, whether they are trained on fixed or variable mesh structures.

Although we focused on shape correspondence in the current paper, it is interesting to explore in future work the use of the dual mesh to define deep networks for other tasks such as shape matching, classification, and semantic segmentation of meshes.

## References

- Bogo F, Romero J, Loper M, Black M (2014) FAUST: Dataset and evaluation for 3D mesh registration. In: CVPR
- Boscaini D, Masci J, Rodolà E, Bronstein M (2016) Learning shape correspondence with anisotropic convolutional neural networks. In: NeurIPS
- Bouritsas G, Bokhnyak S, Ploumpis S, Bronstein M, Zafeiriou S (2019) Neural 3d morphable models: Spiral convolutional networks for 3d shape representation learning and generation. In: ICCV
- Bruna J, Zaremba W, Szlam A, LeCun Y (2014) Spectral networks and locally connected networks on graphs. In: ICLR
- Chen J, Ma T, Xiao C (2018) FastGCN: Fast learning with graph convolutional networks via importance sampling. In: ICLR
- Choy C, Xu D, Gwak JY, Chen K, Savarese S (2016) 3D-R2N2: A unified approach for single and multi-view 3D object reconstruction. In: ECCV
- Clevert D, Unterthiner T, Hochreiter S (2016) Fast and accurate deep network learning by exponential linear units (ELUs). In: ICLR
- Defferrard M, Bresson X, Vandergheynst P (2016) Convolutional neural networks on graphs with fast localized spectral filtering. In: NeurIPS
- Fey M, Lenssen JE (2019) Fast graph representation learning with PyTorch Geometric. In: ICLR Workshop on Representation Learning on Graphs and Manifolds
- Fey M, Lenssen J, Weichert F, Müller H (2018) SplineCNN: Fast geometric deep learning with continuous b-spline kernels. In: CVPR
- Garland M, Heckbert PS (1997) Surface simplification using quadric error metrics. In: Proceedings of the 24th annual conference on Computer graphics and interactive techniques, pp 209–216
- Gong S, Chen L, Bronstein M, Zafeiriou S (2019) Spiralnet++: A fast and highly efficient mesh convolution operator. In: ICCV Workshops
- Guo Y, Wang H, Hu Q, Liu H, Liu L, Bennamoun M (2020) Deep learning for 3d point clouds: A survey. PAMI
- Hanocka R, Hertz A, Fish N, Giryas R, Fleishman S, Cohen-Or D (2019) MeshCNN: a network with an edge. ACM Trans Graphic 38(4):1–12
- He K, Zhang X, Ren S, Sun J (2016) Identity mappings in deep residual networks. In: ECCV
- Hoppe H (1997) View-dependent refinement of progressive meshes. In: Conference on Computer graphics and interactive techniques
- Huang W, Zhang T, Rong Y, Huang J (2018) Adaptive sampling towards fast graph representation learning. In: NeurIPS
- Kingma D, Ba J (2015) Adam: A method for stochastic optimization. In: ICLR
- Kipf T, Welling M (2017) Semi-supervised classification with graph convolutional networks. In: ICLR
- Klokov R, Lempitsky V (2017) Escape from cells: Deep Kd-networks for the recognition of 3D point cloud models. In: ICCV
- Krizhevsky A, Sutskever I, Hinton G (2012) ImageNet classification with deep convolutional neural networks. In: NeurIPS
- Levie R, Monti F, Bresson X, Bronstein MM (2018) Cayleynets: Graph convolutional neural networks with complex rational spectral filters. IEEE Transactions on Signal Processing 67(1):97–109
- Li Y, Bu R, Sun M, Wu W, Di X, Chen B (2018) PointCNN: Convolution on X-transformed points. In: NeurIPS
- Lim I, Dielen A, Campen M, Kobbelt L (2018) A simple approach to intrinsic correspondence learning on unstructured 3d meshes. In: ECCV
- Masci J, Boscaini D, Bronstein M, Vandergheynst P (2015) Geodesic convolutional neural networks on Riemannian manifolds. In: ICCV Workshops
- Maturana D, Scherer S (2015) VoxNet: A 3D convolutional neural network for real-time object recognition. In: IROS
- Milano F, Loquercio A, Rosinol A, Scaramuzza D, Carlone L (2020) Primal-dual mesh convolutional neural networks. In: NeurIPS
- Monti F, Boscaini D, Masci J, Rodolà E, Svoboda J, Bronstein M (2017) Geometric deep learning on graphs and manifolds using mixture model CNNs. In: CVPR
- Qi C, Su H, Mo K, Guibas L (2017a) Pointnet: Deep learning on point sets for 3D classification and segmentation. In: CVPR
- Qi C, Yi L, Su H, Guibas L (2017b) Pointnet++: Deep hierarchical feature learning on point sets in a metric space. In: NeurIPS
- Ranjan A, Bolkart T, Sanyal S, Black MJ (2018) Generating 3d faces using convolutional mesh autoencoders. In: ECCV
- Ren J, Poulernard A, Wonka P, Ovsjanikov M (2018) Continuous and orientation-preserving correspondences via functional maps. ACM Transactions on Graphics (TOG) 37(6):1–16
- Riegler G, Ulusoy A, Geiger A (2017) OctNet: Learning deep 3D representations at high resolutions. In: CVPR
- Sen P, Namata G, Bilgic M, Getoor L, Galligher B, Eliassi-Rad T (2008) Collective classification in network data. AI magazine 29(3):93–93
- Simonovsky M, Komodakis N (2017) Dynamic edge-conditioned filters in convolutional neural networks on graphs. In: CVPR
- Simonyan K, Zisserman A (2015) Very deep convolutional networks for large-scale image recognition. In: ICLR
- Srivastava N, Hinton G, Krizhevsky A, Sutskever I, Salakhutdinov R (2014) Dropout: A simple way to prevent neural networks from overfitting. JMLR

- Tatarchenko M, Dosovitskiy A, Brox T (2017) Octree generating networks: Efficient convolutional architectures for high-resolution 3D outputs. In: ICCV
- Tombari F, Salti S, Stefano LD (2010) Unique signatures of histograms for local surface description. In: ECCV
- Veličković P, Cucurull G, Casanova A, Romero A, Liò P, Bengio Y (2018) Graph attention networks. In: ICLR
- Verma N, Boyer E, Verbeek J (2018) FeaStNet: Feature-steered graph convolutions for 3D shape analysis. In: CVPR
- Wang Y, Sun Y, Liu Z, Sarma SE, Bronstein MM, Solomon JM (2019) Dynamic graph cnn for learning on point clouds. *ACM Transactions on Graphics (TOG)* 38(5):1–12
- Wu Z, Pan S, Chen F, Long G, Zhang C, Philip SY (2020) A comprehensive survey on graph neural networks. *IEEE Transactions on Neural Networks and Learning Systems*
- Yan DM, Bao G, Zhang X, Wonka P (2014) Low-resolution remeshing using the localized restricted voronoi diagram. *IEEE transactions on visualization and computer graphics* 20(10):1418–1427
- Zhang S, Tong H, Xu J, Maciejewski R (2019) Graph convolutional networks: a comprehensive review. *Computational Social Networks* 6(1):11